Eur. Phys. J. C (2023) 83:1064
https://doi.org/10.1140/epjc/s10052-023-12224-0

THE EUROPEAN PHYSICAL JOURNAL C

Regular Article - Theoretical Physics

Probability measures of fermions on branes

A. R. P. Moreira[1,2,a], **Shi-Hai Dong**[1,3,b]

[1] Research Center for Quantum Physics, Huzhou University, Huzhou 313000, People's Republic of China
[2] Secretaria da Educação do Ceará (SEDUC), Coordenadoria Regional de Desenvolvimento da Educaão (CREDE 9), Horizonte, Ceará 62880-384, Brazil
[3] Centro de Investigación en Computación, Instituto Politécnico Nacional, UPALM, Mexico City 07700, Mexico

Received: 19 October 2023 / Accepted: 6 November 2023 / Published online: 20 November 2023

Abstract In our research, we explore the impact of a geometric non-minimal coupling between fermions and curvature scalars on the positioning of fermions within a brane structure. Our investigation encompasses massless fermionic modes and massive modes, revealing that specifically fermionic modes with left chirality are situated within the brane. This insight allows us to gain a more direct understanding of how the system's geometry influences the placement of fermion fields on the brane. To delve deeper into the precise localization of massless fermionic modes, we employ entropic information measurements. By varying the parameters that govern the curvature scalars, we observe the ability to adjust the localization of these fermionic modes on the brane. Importantly, the BBM uncertainty relation remains satisfied in all scenarios, particularly for $f_{1,2,3}$. We leverage the Shannon entropy as a highly effective metric to yield accurate results regarding the positioning of massless fermionic modes within our model. In the case of massive fermionic modes, we utilize relative probability analysis to pinpoint the resonant modes, and we identify the existence of these resonant modes in both $f_{1,2,3}$ cases. Ultimately, we ascertain that these parameters influence the placement of resonant modes by increasing the amplitude of the massive modes in the core of the brane.

1 Introduction

The study of modified gravity models has gained significant attention in recent times due to the limitations of General Relativity (GR). One of these early limitations was observed by Smith [1] and Zwicky [2], who noticed the existence of an unknown invisible matter, commonly referred to as dark matter, responsible for holding galaxy clusters together. The existence of dark matter has been substantiated through phenomena such as gravitational lensing [3,4], which is caused by the deviation of light paths due to intense gravitational fields. Another substantial gap in our understanding emerged when the accelerated expansion of the universe was confirmed [5–8]. Furthermore, the large disparity between the Planck scale and the electroweak scale, known as the hierarchy problem, continues to challenge our comprehension of fundamental physics [9,10].

In recent years, the research landscape has seen a proliferation of modified gravitational models. One such model is the $f(R)$ gravity, which extends GR [11,12]. The $f(R)$ gravity has shown its capability to generalize GR, yielding noteworthy outcomes in areas like the study of black hole solutions [13–18], dark energy [19,20], universe acceleration [21], and its effectiveness on cosmological scales. However, it falls short of accurately matching the observed data related to the rotation of spiral galaxies [22,23] and the regime data of the solar system [24]. These discrepancies have prompted the exploration of new extensions of GR, such as $f(R,\mathcal{T})$ [25–28] and $f(R, R_{\mu\nu}R^{\mu\nu})$ [29–31].

Simultaneously, the braneworld scenario has piqued the curiosity of many researchers [9,10]. This model offers the potential to address the limitations of GR, including the hierarchy problem [10], the nature of dark matter [32], the cosmological constant problem [33], and more. What makes this model intriguing is that it confines all matter fields of the standard model to the brane (our three-dimensional space), while gravity is the only force that can propagate through the bulk (extra dimensions). Consequently, substantial interest has been invested in understanding how matter fields are localized on the brane [34–50].

The localization of fermions on the brane is of particular interest, offering potential experimental verification of

[a] e-mail: allan.moreira@fisica.ufc.br (corresponding author)
[b] e-mail: dongsh2@yahoo.com

the existence of extra dimensions. This topic has been extensively studied [51–65]. Numerous mechanisms for localizing fermions on the brane have been proposed, many of which are inspired by the conventional Yukawa-like coupling between fermion fields and background scalar fields. Additionally, new localization mechanisms have emerged, such as non-minimal coupling between fermions and curvature [66,67], torsion [68], and non-metricity [69]. These couplings demonstrate how geometry can more directly influence the localization of fermion fields on the brane. This naturally leads to questions about the potential impact of other types of geometric couplings, specifically those related to curvature scalars (e.g., R - curvature scalar, $R_{\mu\nu}$ – Ricci tensor, $R_{\mu\nu\lambda\sigma}$ – Riemann tensor).

In this work, we explore how curvature scalars influence the localization of a 1/2 spin fermion on the brane. To this end, we calculate various probability measures, including information entropy for massless fermion modes and resonant modes among the massive modes. The structure of this work is as follows: In Sect. 2, we introduce the mechanism for localizing fermions on the brane and examine both massless and massive mode solutions. Section 3 delves into probability measures, and in the final Sect. 4, we provide concluding remarks and outline future perspectives.

2 Location of fermion

In this section, we delve into the localization conditions for fermion fields on the brane. Our focus is on examining the spinor sector with spin 1/2 residing on the brane. To understand the localization of these fermions on the brane, we introduce a novel geometric coupling between the spinor field and the scalar fields that define the curvature, specifically, the curvature scalar (R) and its higher-order counterparts ($R_{MN}R^{MN}$ and $R_{MNPQ}R^{MNPQ}$). Consequently, we extend the fifth-dimensional action for a Dirac fermion by incorporating a non-minimal coupling with these curvature-related terms, resulting in the following action:

$$\mathcal{S}_{1/2} = \int \sqrt{-g}\overline{\Psi}\Big[\Gamma^M D_M\Psi - \xi\Gamma^M\partial_M F(R, R_{MN}R^{MN}, R_{MNPQ}R^{MNPQ})\Psi\Big]d^5x, \tag{1}$$

where g is the determinant of the metric and $D_M = \partial_M + \Omega_M$ is the covariant derivative. The Ω_M appearing in D_M is the spin connection

$$\Omega_M = \frac{1}{4}\Big(\Omega_M{}^{\overline{MN}}\Big)\,\Gamma_{\overline{M}}\Gamma_{\overline{N}}, \tag{2}$$

with

$$\Omega_M{}^{\overline{MN}} = \frac{1}{2}E^{N\overline{M}}(\partial_M E_N^{\overline{N}} - \partial_N E_M^{\overline{N}}) - \frac{1}{2}E^{N\overline{N}}(\partial_M E_N^{\overline{M}} - \partial_N E_M^{\overline{M}}) - \frac{1}{2}E^{P\overline{M}}E^{Q\overline{N}}E_M^{\overline{R}}(\partial_P E_{Q\overline{R}} - \partial_Q E_{P\overline{R}}), \tag{3}$$

where $\Gamma^{\overline{M}}$ is the plane Dirac matrices and $E_M^{\overline{M}}$ are the vielbeins that define the tangent space

$$g_{MN} = \eta_{\overline{MN}}E_M^{\overline{M}}E_N^{\overline{N}}. \tag{4}$$

The indices M span the coordinates in the bulk, ranging from 0 to $D-1$, while the barred indices $\overline{M}$ cover the coordinates of the tangent space within the same range. Additionally, the Clifford algebra is followed, satisfying $\{\Gamma^M, \Gamma^N\} = 2g^{MN}$, where the curved Dirac matrices Γ^M are constructed as $\Gamma^M = E_{\overline{M}}^M\Gamma^{\overline{M}}$.

The metric $ds^2 = e^{2A(y)}\eta_{\mu\nu}dx^\mu dx^\nu + dy^2$ defines the braneworld scenario, where $\eta_{\mu\nu} = (-1, 1, 1, 1)$ represents the Minkowski metric, characterizing the space where we reside. The warp factor, denoted as $e^{A(y)}$, exerts control over the thickness of the brane, while y denotes the extra dimension. Employing a coordinate transformation, namely, $dz = e^{-A(y)}dy$, the metric given above can be expressed in the following form: $ds^2 = e^{2A}(\eta^{\mu\nu}dx^\mu dx^\nu + dz^2)$.

Thus, the spin connection to the model is given by

$$\Omega_\mu = \frac{1}{2}(\partial_z A)\gamma_\mu\gamma_4 \;\text{ end }\; \Omega_z = 0, \tag{5}$$

which leads us to the Dirac equation

$$\Big[\gamma^\mu\partial_\mu + \gamma^4(\partial_z + 2\partial_z A) - \xi e^A\partial_z F\Big]\Psi = 0, \tag{6}$$

where $F = F(R, R_{MN}R^{MN}, R_{MNPQ}R^{MNPQ})$ for simplicity.

With spinor decomposition

$$\Psi = \sum_n [\psi_{L,n}(x)\varphi_{L,n}(z) + \psi_{R,n}(x)\varphi_{R,n}(z)]e^{-2A}, \tag{7}$$

we fall back on the coupled equations

$$\Big[\partial_z - \xi\,\partial_z F\Big]\varphi_{L,n}(z) = m_n\varphi_{R,n}(z),$$
$$\Big[\partial_z + \xi\,\partial_z F\Big]\varphi_{R,n}(z) = -m_n\varphi_{L,n}(z), \tag{8}$$

where $\gamma^4\psi_{R,L} = \pm\psi_{R,L}$ and $\gamma^\mu\partial_\mu\psi_{R,L} = m\psi_{L,R}$.

The Eq. (8) can be easily decoupled, arriving at Schrödinger-like equations

$$\Big[-\partial_z^2 + V_{L,n}(z)\Big]\varphi_{L,n}(z) = m_n^2\varphi_{L,n}(z),$$
$$\Big[-\partial_z^2 + V_{R,n}(z)\Big]\varphi_{R,n}(z) = m_n^2\varphi_{R,n}(z), \tag{9}$$

where the effective potentials are

$$V_{L,R}(z) = U^2 \pm \partial_z U, \tag{10}$$

being $U = \xi\,\partial_z F$.

It is worth noting that the orthonormality condition is satisfied

$$\int \varphi_{R,p}\varphi_{R,n}dz = \int \varphi_{L,p}\varphi_{L,n}dz = \delta_{pn}\int \varphi_{L,p}\varphi_{R,n}dz = 0, \tag{11}$$

which is the case with Yukawa's usual coupling. Furthermore, the massless modes are defined as

$$\varphi_{L0,R0}(z) \propto \exp\left[\pm\int \xi\,\partial_z F dz\right] = \exp\left[\pm\xi F\right]. \tag{12}$$

Finally, we can further simplify our choice of function F by making $F = \ln[f(R, R_{MN}R^{MN}, R_{MNPQ}R^{MNPQ})]$, which takes us to modes without mass in form

$$\varphi_{L0,R0}(z) \propto f^{\pm\xi}. \tag{13}$$

For these fermionic zero modes to be localized, the normalization condition must be obeyed, i.e.,

$$\int \varphi_{R0,L0}(z)^2 dz < \infty. \tag{14}$$

For this to happen, the curvature function f must meet some conditions. Firstly, the function f must go to zero asymptotically ($f|_{z\to\pm\infty} \to 0$). Furthermore, the superpotential U must go to zero in a vacuum, i.e., $U(f)|_{z\to\pm\infty} \to 0\,(\xi > 0)$.

Regarding the massive modes, numerical methods are the only means of obtaining their solutions. For this, we propose the boundary conditions [51,56,57]

$$\begin{aligned} &\varphi_{even}(0) = c, \quad \partial_z\varphi_{even}(0) = 0,\\ &\varphi_{odd}(0) = 0, \quad \partial_z\varphi_{odd}(0) = c. \end{aligned} \tag{15}$$

The boundary conditions (15) guarantee that massive solutions $\varphi_{L,R}(z)$ will be even φ_{even} or odd φ_{odd} wave functions.

Now, the only task left is to define the specific form of the functions f. We will proceed by examining three distinct cases, with the first case being

$$f_1 = \frac{3\alpha(R+28) + 4\beta(\sqrt{6R_{MNPQ}R^{MNPQ} - 3R_{MN}R^{MN}} - 6)}{84\alpha - 24\beta}, \tag{16}$$

second case being

$$f_2 = \frac{9^\beta R^\alpha 28^{\beta-\alpha} + (-1)^{\alpha-1}(R_{MN}R^{MN} + R_{MNPQ}R^{MNPQ})^\beta}{(-1)^\alpha(R_{MN}R^{MN} + R_{MNPQ}R^{MNPQ})^\beta}, \tag{17}$$

and the third case being

$$f_3 = \frac{\alpha(R+28) + \beta(R_{MN}R^{MN} - 164) + \sigma(R_{MNPQ}R^{MNPQ} - 88)}{28\alpha - 164\beta - 88\sigma}. \tag{18}$$

In particular, the choice of these functions, characterized by the constants α, β, and σ, is motivated by their ability to satisfy the necessary conditions for normalizing zero fermionic modes. Moreover, these functions offer simplicity and efficiency, making them well-suited for the purpose of this study.

As we are interested in investigating a thick brane scenario, we take the ansatz [34]

$$e^{2A(y)} = \cosh^{-2p}(\lambda y), \tag{19}$$

where the parameters p and λ control the thickness of the brane.

2.1 First case

The selection of $f = f_1$ as our first choice is particularly intriguing due to the fact that the effective potential (10) remains independent of the parameters influencing the curvature constants (α and β). Notably, the behavior of this effective potential is indicative of its ability to accommodate well-localized massless modes (as depicted in Fig. 1a). Additionally, the massive modes exhibit a behavior resembling free waves in their asymptotic regions (as illustrated in Fig. 1b, c). It's worth noting that, for certain specific mass values, the amplitude of the massive modes displays more pronounced characteristics near the brane origin, suggesting the presence of potential resonant modes.

Conversely, the massless modes exhibit sensitivity to the curvature parameters. As we manipulate the value of α, which governs the impact of the curvature scalar, we observe an increase in the amplitude of the massless mode (as seen in Fig. 2a). Conversely, when we augment the value of the parameter β" (as represented in Fig. 2b), we witness a contrasting effect, leading to a reduction in the amplitude of the massless mode.

2.2 Second case

In the case of f_2, the effective potential exhibits intriguing characteristics. As we increment the value of α, the potential reveals the emergence of additional peaks and wells, as depicted in Fig. 3a. This behavior directly impacts the massless modes, causing them to exhibit attempts to split into new peaks near the brane origin, as visualized in Fig. 3c. On the other hand, when we manipulate the β parameter, the potential exhibits an augmentation of the potential barriers in the vicinity of the origin, leading to the localization of massless modes, as illustrated in Fig. 3b, d.

The behavior of massive modes is also influenced by the changes in the effective potential. As we adjust the parameter α, the oscillations' amplitudes tend to approach the core of the brane, accompanied by a reduction in amplitude, as demonstrated in Fig. 4a, b. Conversely, when we increase the

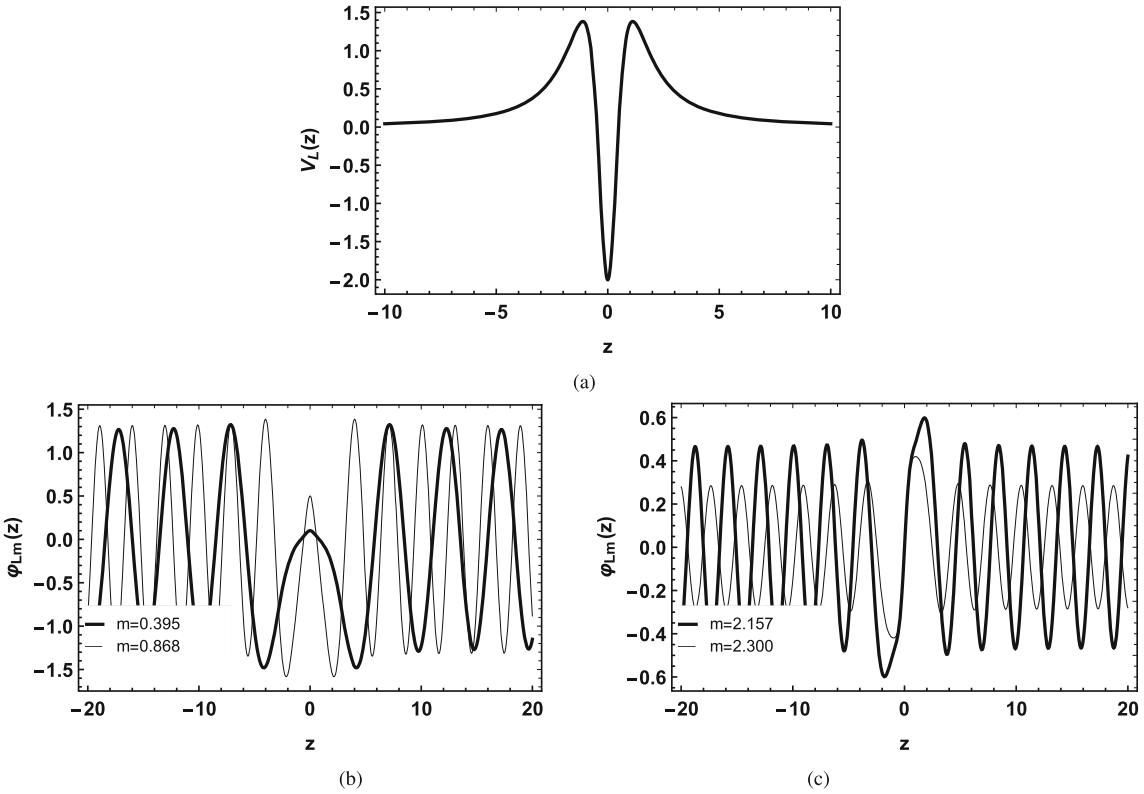

Fig. 1 For the first case f_1 with $\xi = p = \lambda = 1$. **a** Effective potential $V_R(z)$. Massive modes **b** even and **c** odd

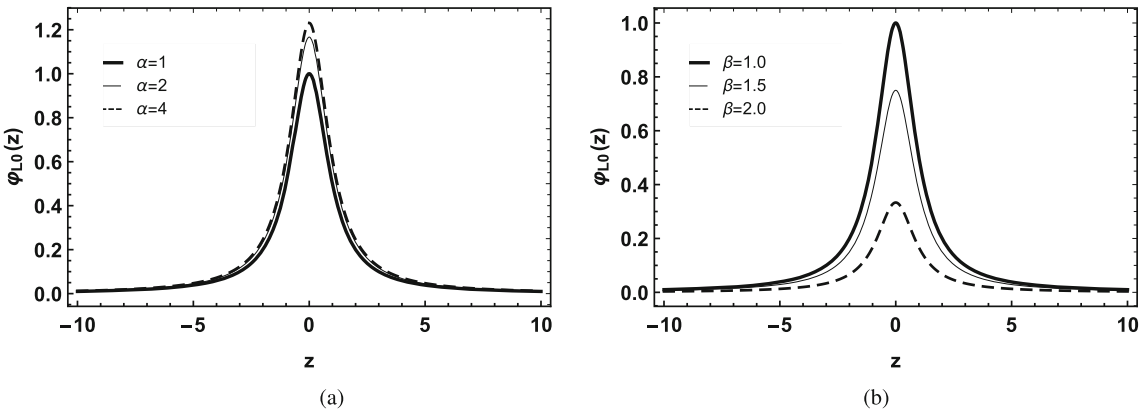

Fig. 2 Massless modes for f_1 with $\xi = p = \lambda = 1$. **a** Being $\beta = 1$ and varying α. **b** Being $\alpha = 1$ and varying β

value of β, the oscillation amplitudes become larger, leading them to move away from the origin, as depicted in Fig. 4c, d.

2.3 Third case

The case of f_3 presents a more general expression, allowing us to analyze the individual influence of each curvature constant on the fermion's location. As the parameter α is increased, the potential barriers and wells become larger (Fig. 5a). This results in massless modes tending to split into two peaks at the brane origin (Fig. 5b). Similar effects occur when we increase the values of the parameters β (Fig. 5c, d) and σ (Fig. 5e, f).

Something intriguing happens with the massive modes. Increasing the value of α causes the double peak located at the origin to merge into a single peak with a more pronounced amplitude (Fig. 6a). Simultaneously, oscillations outside the core tend to decrease their amplitudes (Fig. 6a, b). A similar effect is observed when we increase the value of β (Fig. 6c, d) and σ (Fig. 6e, f). Notably, as these curvature parameters are increased, the oscillations approach the brane core.

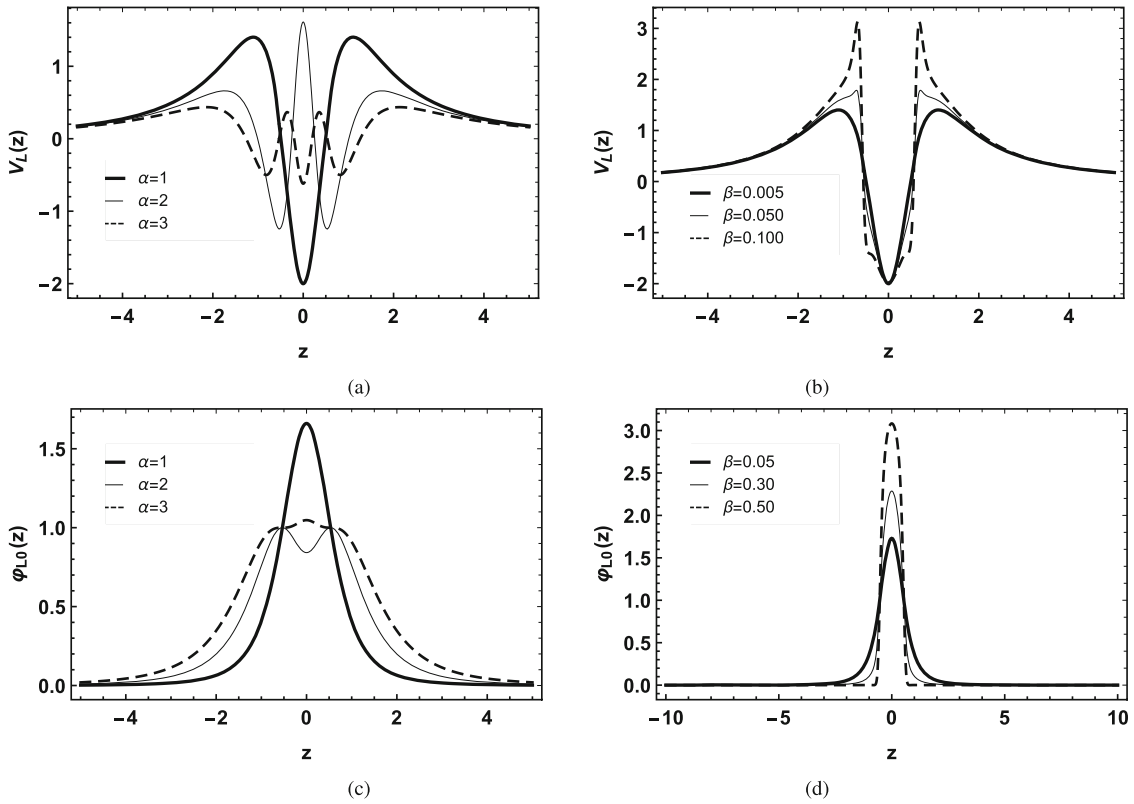

Fig. 3 For the first case f_2 with $\xi = p = \lambda = 1$. Where $\beta = 0.05$ **a** effective potential and **c** massless mode. Where $\alpha = 1$ **b** effective potential and **d** massless mode

3 Probability measures

3.1 Information entropy

The massless fermionic modes are effectively localized on the brane, facilitating the application of probability measures to examine the impact of the $f_{1,2,3}$ functions on their positions. A commonly employed probability measure for investigating the location of fermionic particles in various physical scenarios is the well-known Shannon entropy. This information theory, introduced by Shannon in 1948 [70], was initially designed to study the transmission of information between a source and a receiver. However, given its derivation from the probability densities of a system, Shannon entropy can also be applied to quantum systems. Consequently, we will explore the Shannon entropy for the massless fermionic modes in our brane scenario.

Shannon entropy is defined as

$$S_z = -\int_{-\infty}^{\infty} |\varphi_{L0,R0}(z)|^2 \ln |\varphi_{L0,R0}(z)|^2 dz. \tag{20}$$

We also need this entropic measure in the reciprocal space of the system (momentum space),

$$S_{p_z} = -\int_{-\infty}^{\infty} |\varphi_{L0,R0}(p_z)|^2 \ln |\varphi_{L0,R0}(p_z)|^2 dz, \tag{21}$$

which is defined through the conventional Fourier transform

$$|\varphi_{L0,R0}(p_z)|^2 = \frac{1}{\sqrt{2\pi}} \int_{-\infty}^{\infty} |\varphi_{L0,R0}(z)|^2 \, \mathrm{e}^{-ipz} dz. \tag{22}$$

Similar to Heisenberg's uncertainty principle, a new uncertainty relationship between entropic information measures was obtained by Beckner, Bialynicki-Birula, and Mycielski (BBM) [71,72]

$$S_z + S_{p_z} \geq D(1 + \ln\pi), \tag{23}$$

where D represents the dimension that senses the modifications of the information measures. In our case, only the extra dimension is related to the location of the fermionic modes, thus $D = 1$.

Since we are dealing with probability densities, it is imperative to normalize the massless mode solutions. For the f_1 scenario, the information measures remain unaffected by variations in α and β. The entropic measure is found to be $S_z = 1.22417$. Reciprocally, in momentum space, the entropic measure is $S_{p_z} = 0.99961$. In this case, the total entropic measure for the system, which is given by $S_z + S_{p_z}$, equals 2.22378. This value is greater than $1 + \ln\pi$, thus satisfying the BBM uncertainty relation.

For the f_2 scenario, we conduct an analysis of the information measures as presented in Table 1. It's worth noting

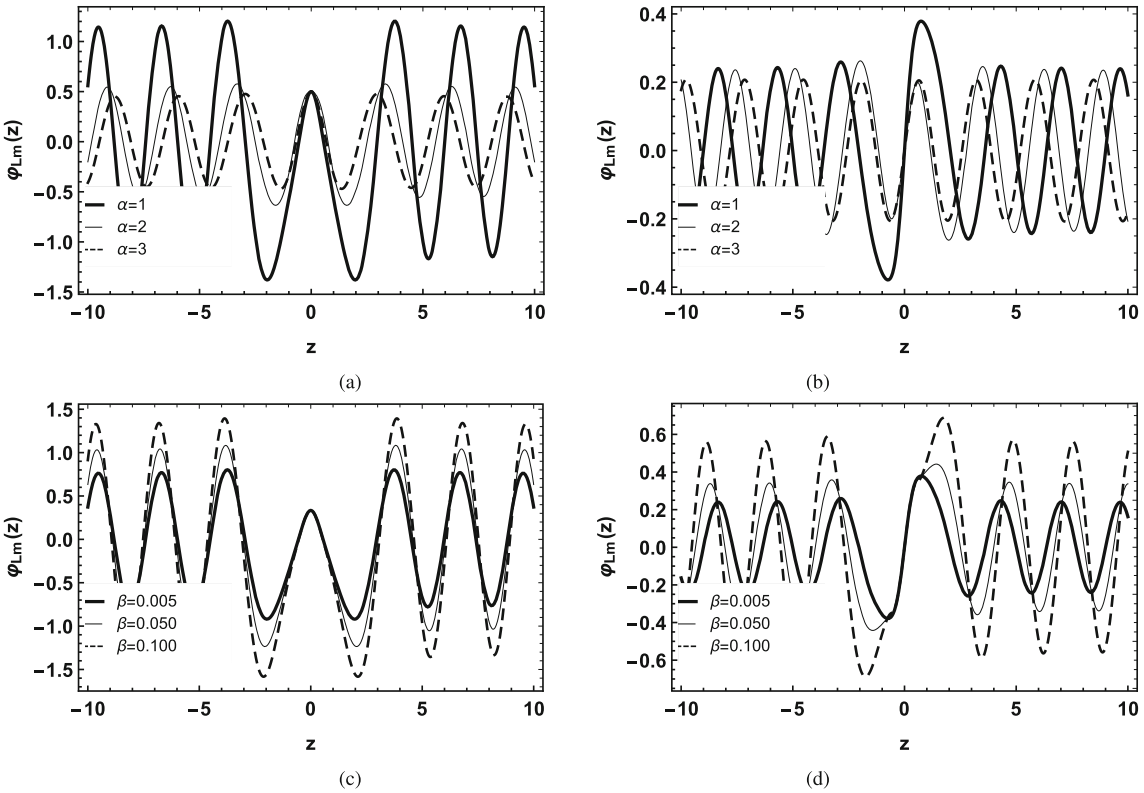

Fig. 4 Massive modes for f_2 with $\xi = p = \lambda = 1$. Being $\beta = 0.005$ **a** even with $m = 0.644$ and **b** odd with $m = 2.439$. Being $\alpha = 1$ **c** even with $m = 0.644$ and **d** odd with $m = 2.439$

Table 1 Numerical result of the Shannon's entropy for f_2 with $\xi = p = \lambda = 1$

α	β	S_z	S_{p_z}	$S_z + S_{p_z}$	$1 + \ln \pi$
1	1	0.89619	2.71706	3.61326	
2	1	1.23600	1.53740	2.77341	2.14473
4	1	1.69294	0.51960	2.21255	
1	1	0.89619	2.71706	3.61326	
1	0	1.22417	0.99999	2.22417	2.14473
1	−1	1.92269	0.28216	2.20486	

that an increase in the value of α leads to an increase in the information measures. This signifies less certainty regarding the location of these massless fermionic modes with higher values of the α parameter. On the contrary, entropic measures decrease, indicating greater certainty in reciprocal space. Conversely, when we increase the value of β, the opposite trend is observed. In this case, the entropy S_z decreases, while the entropy S_{p_z} increases. Simultaneously, the total entropy of the system increases, which results in increased uncertainties regarding the location of these massless modes on the brane. These observations highlight the sensitivity of the system's information measures to variations in the parameters α and β, underlining the complexity of the relationship between these parameters and the localization of massless fermionic modes.

For the f_3 scenario, we present an analysis of the information measures in Table 2. It's evident that as we increase the values of the parameters α, β, and σ, the information measures S_z also increase. This increase implies a greater degree of uncertainty regarding the location of these fermionic modes in z-space. Simultaneously, the information measures in reciprocal space S_{p_z} decrease as these parameters increase, indicating a reduction in uncertainty regarding the location of these fermionic modes in p_z space. Consequently, the total entropic measurement of the system, represented by $S_z + S_{p_z}$, increases. This increase signifies a greater degree of uncertainty in the location of massless modes on the brane, implying a delocalization process. These observations highlight the complex interplay between the parameters α, β, and σ, and their impact on the localization and uncertainty of massless fermionic modes in the system.

3.2 Resonate modes

To calculate probability measures for non-localized modes, we introduce the study of resonant modes, which enables a more in-depth analysis of the system. This approach is particularly useful for massive modes, which exhibit non-localized behavior.

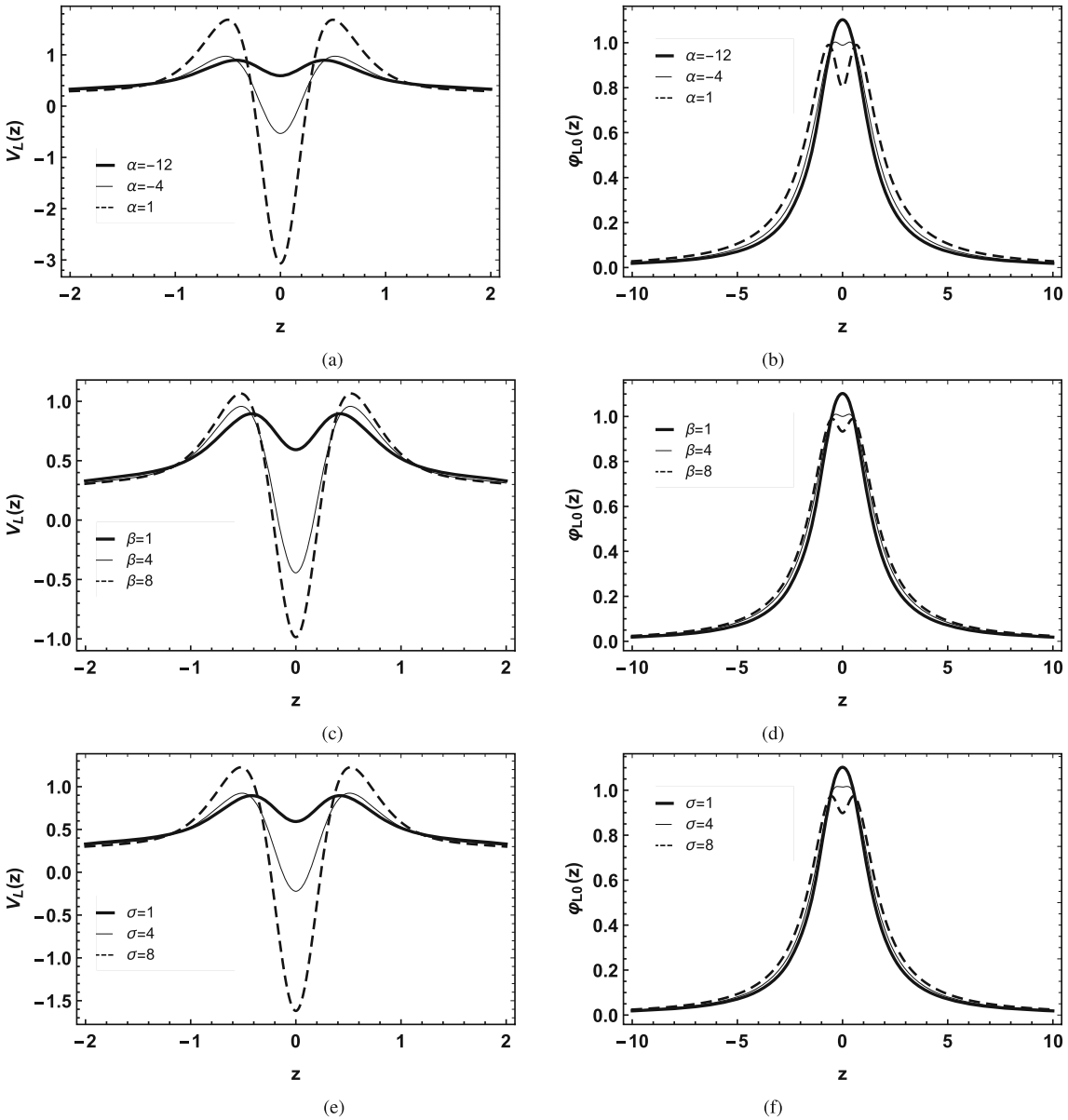

Fig. 5 For the first case f_3 with $\xi = p = \lambda = 1$. Where $\beta = \sigma = 1$ **a** effective potential and **b** massless mode. Where $\alpha = -12$ and $\sigma = 1$ **c** effective potential and **d** massless mode. Where $\alpha = -12$ and $\beta = 1$ **e** effective potential and **f** massless mode

Among all the massive modes, we select resonant modes based on their characteristics, specifically focusing on those with the highest amplitudes near the brane core. These resonant modes represent configurations with a high likelihood of the massive fermion being located within the brane. To identify these resonant modes, we compute relative probabilities [57,73]

$$P(m) = \frac{\int_{-z_b}^{z_b} |\varphi_{L,R}(z)|^2 dz}{\int_{-z_{max}}^{z_{max}} |\varphi_{L,R}(z)|^2 dz}. \tag{24}$$

This probability measures the chance of finding a particle of mass m in a narrow band $2z_b$. Here, z_{max} represents the limit of the domain, and the smaller the value of the parameter z_b, the easier it becomes to identify the probability peaks that represent the resonant modes.

The extensive analysis of the three mentioned cases in the previous section, involving the massive modes denoted as $f_{1,2,3}$, reveals a striking asymptotic free wave behavior. This observation strongly suggests that fermions have indeed escaped from the brane. However, it is noteworthy that certain mass eigenvalues result in massive wave eigenfunctions with a pronounced amplitude concentrated at the origin. This phenomenon implies a significant probability of locating these fermions on the brane, despite the theoretical potential for tunneling out of it. In the case of f_1, the resonant modes find clear representation in the form of peaks visible in the rel-

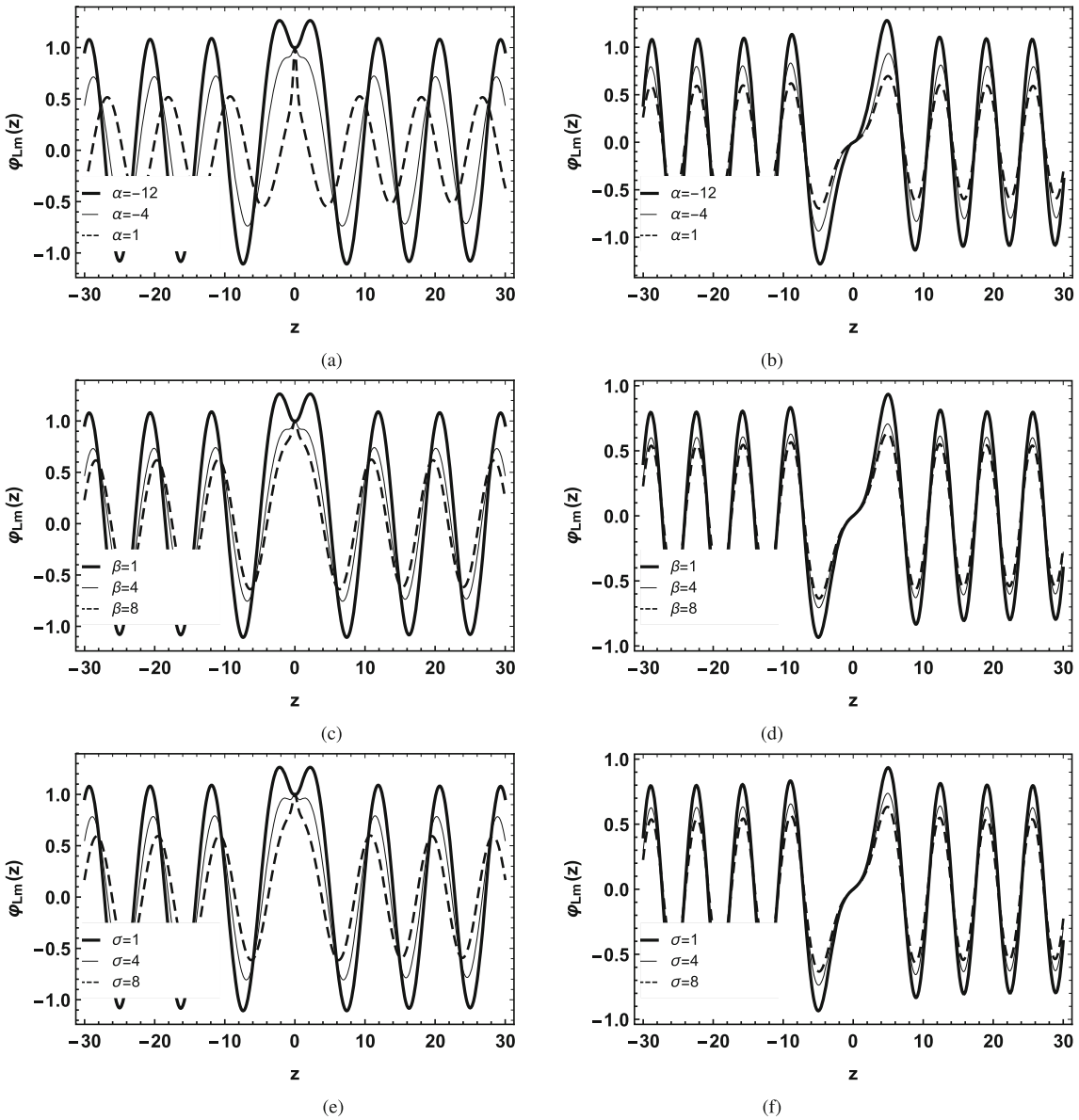

Fig. 6 Massive modes for f_3 with $\xi = p = \lambda = 1$. Being $\beta = \sigma = 1$ **a** even with $m = 1.483$ and **b** odd with $m = 2.302$. Being $\alpha = -12$ and $\sigma = 1$ **c** even with $m = 1.483$ and **d** odd with $m = 2.302$. Being $\alpha = -12$ and $\beta = 1$ **e** even with $m = 1.483$ and **f** odd with $m = 2.302$

ative probability plot (Fig. 7). Similarly, for both f_2 (Fig. 8) and f_3 (Fig. 9), the resonant modes are distinctly manifested as peaks, reinforcing the intriguing possibility of fermionic presence on the brane even amidst the high likelihood of tunneling away from it.

4 Final remarks

In this research, we investigate the impact of a geometric non-minimal coupling between fermions and curvature scalars (specifically R, $R_{\mu\nu}$, and $R_{\mu\nu\lambda\sigma}$) on the positioning of fermions within the brane. To achieve this, we examine three distinct coupling cases denoted as $f_{1,2,3}$, characterized by the function $f(R, R_{MN}R^{MN}, R_{MNPQ}R^{MNPQ})$. Our analysis reveals the existence of both massless and massive fermionic modes. An intriguing discovery is that only fermionic modes with left chirality are found to be localized on the brane. Additionally, we gain a deeper understanding of how the system's geometry directly influences the placement of fermion fields within the brane.

For a more precise investigation of the localization of massless fermionic modes, we employ entropic information measurements. Our findings indicate that by adjusting the parameters governing the curvature scalars (α, β, and σ), we have the ability to control the extent of localization of these

Table 2 Numerical result of the Shannon's entropy for f_3 with $\xi = p = \lambda = 1$

α	β	σ	S_z	S_{p_z}	$S_z + S_{p_z}$	$1 + \ln \pi$
-12	1	1	1.50051	0.71311	2.21363	
-4	1	1	1.63656	0.57969	2.21625	2.14473
1	1	1	1.79453	0.43766	2.23219	
-12	1	1	1.50051	0.71311	2.21363	
-12	4	1	1.62783	0.58534	2.21318	2.14473
-12	12	1	1.69685	0.51538	2.21224	
-12	1	1	1.50051	0.71311	2.21363	
-12	1	4	1.60468	0.60962	2.21430	2.14473
-12	1	18	1.71714	0.49734	2.21448	

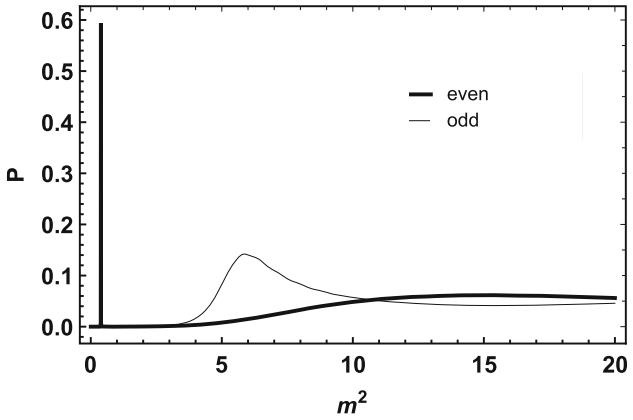

Fig. 7 Relative probability for f_1 with $\xi = p = \lambda = 1$

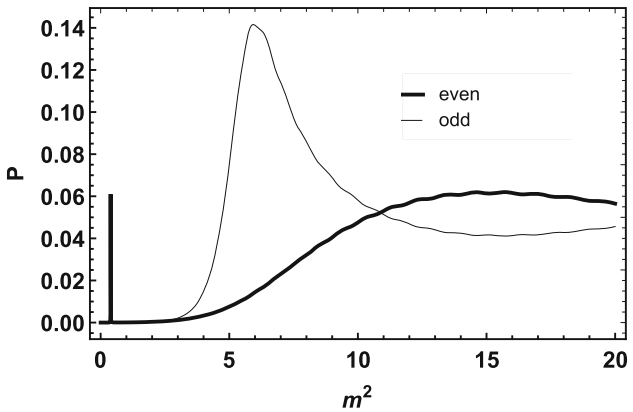

Fig. 8 Relative probability for f_2 with $\xi = p = \lambda = \alpha = 1$ and $\beta = 0.005$

fermionic modes on the brane. Remarkably, the BBM uncertainty relation is satisfied in all instances of $f_{1,2,3}$. To the best of our knowledge, this is the first study to utilize Shannon entropy as a tool for assessing the localization of fermions on the brane, and it has proven to be highly effective in providing accurate results regarding the placement of massless fermionic modes in our model.

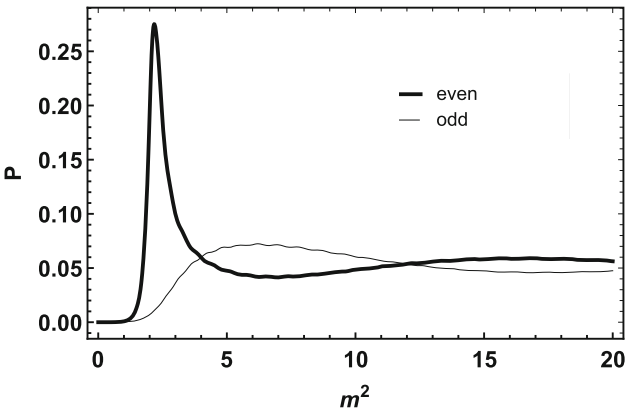

Fig. 9 Relative probability for f_3 with $\xi = p = \lambda = 1 = \beta = \sigma = 1$ and $\alpha = -12$

In our exploration of massive fermionic modes, we employ relative probability to identify resonant modes, which are characterized by higher amplitudes near the brane core, indicating a greater likelihood of being located on the brane. We ascertain the presence of these resonant modes in both $f_{1,2,3}$, and we further observe that by manipulating the curvature parameters (α, β, and σ), we can enhance the amplitude of the massive modes at the brane core, thus demonstrating the significant influence of these parameters on the localization of resonant modes.

Acknowledgements One of the authors S.H. Dong would like to thank the partial support of project 20230316-SIP-IPN, Mexico. S.H. Dong started this work on the leave of IPN due to permission of research stay in China.

Data availability This manuscript has no associated data or the data will not be deposited. [Authors' comment: The datasets generated during and/or analysed during the current study are available from the corresponding author on reasonable request.]

Funded by SCOAP[3]. SCOAP[3] supports the goals of the International Year of Basic Sciences for Sustainable Development.

References

1. S. Smith, Astrophys. J. **83**, 23–30 (1936)
2. F. Zwicky, Astrophys. J. **86**, 217–246 (1937)

3. B. Patel, C. McCully, S.W. Jha, S.A. Rodney, D.O. Jones, O. Graur, J. Merten, A. Zitrin, A.G. Riess, T. Matheson et al., Astrophys. J. **786**, 9 (2014)
4. R. Massey, T. Kitching, J. Richard, Rep. Prog. Phys. **73**, 086901 (2010)
5. S. Perlmutter et al. [Supernova Cosmology Project], Astrophys. J. **517**, 565–586 (1999)
6. A.G. Riess, A.V. Filippenko, W. Li, R.R. Treffers, B.P. Schmidt, Y. Qiu, J. Hu, M. Armstrong, C. Faranda, E. Thouvenot, Astron. J. **118**, 2675–2688 (1999)
7. S. Gonzalez-Gaitan, A. Conley, F.B. Bianco, D.A. Howell, M. Sullivan, K. Perrett, R. Carlberg, P. Astier, D. Balam, C. Balland et al., Astrophys. J. **745**, 44 (2012)
8. M. Ganeshalingam, W. Li, A.V. Filippenko, Mon. Not. R. Astron. Soc. **416**, 2607 (2011)
9. L. Randall, R. Sundrum, Phys. Rev. Lett. **83**, 4690 (1999)
10. L. Randall, R. Sundrum, Phys. Rev. Lett. **83**, 3370 (1999)
11. A. De Felice, S. Tsujikawa, Living Rev. Relativ. **13**, 3 (2010)
12. S. Nojiri, S. Odintsov, Phys. Rep. **505**, 59 (2011)
13. L. Sebastiani, S. Zerbini, Eur. Phys. J. C **71**, 1591 (2011)
14. T. Multamaki, I. Vilja, Phys. Rev. D **74**, 064022 (2006)
15. S.H. Hendi, B. Eslam Panah, R. Saffari, Int. J. Mod. Phys. D **23**(11), 1450088 (2014)
16. G.G.L. Nashed, E.N. Saridakis, Phys. Rev. D **102**(12), 124072 (2020)
17. G.G.L. Nashed, S. Nojiri, Phys. Lett. B **820**, 136475 (2021)
18. Z.Y. Tang, B. Wang, E. Papantonopoulos, Eur. Phys. J. C **81**(4), 346 (2021)
19. S. Nojiri, S.D. Odintsov, Phys. Rev. D **74**, 086005 (2006)
20. S. Tsujikawa, Phys. Rev. D **77**, 023507 (2008)
21. M.Z. Mughal, I. Ahmad, Gravit. Cosmol. **28**(1), 37–58 (2022)
22. T. Chiba, Phys. Lett. B **575**, 1–3 (2003)
23. G.J. Olmo, Phys. Rev. D **72**, 083505 (2005)
24. A.L. Erickcek, T.L. Smith, M. Kamionkowski, Phys. Rev. D **74**, 121501 (2006)
25. B.M. Gu, B. Guo, H. Yu, Y.X. Liu, Phys. Rev. D **92**(2), 024011 (2015)
26. D. Bazeia, A.S. Lobão, EPL **136**(6), 61002 (2021)
27. D. Deb, F. Rahaman, S. Ray, B.K. Guha, Phys. Rev. D **97**(8), 084026 (2018)
28. P.H.R.S. Moraes, R.A.C. Correa, R.V. Lobato, JCAP **07**, 029 (2017)
29. G.J. Olmo, D. Rubiera-Garcia, Phys. Rev. D **86**, 044014 (2012)
30. G.J. Olmo, D. Rubiera-Garcia, Int. J. Mod. Phys. D **21**, 1250067 (2012)
31. G.J. Olmo, D. Rubiera-Garcia, Eur. Phys. J. C **72**, 2098 (2012)
32. T. Gherghetta, B. von Harling, JHEP **1004**, 039 (2010)
33. J.M. Schwindt, C. Wetterich, Nucl. Phys. B **726**, 75 (2005)
34. M. Gremm, Phys. Lett. B **478**, 434–438 (2000)
35. O. Castillo-Felisola, A. Melfo, N. Pantoja, A. Ramirez, Phys. Rev. D **70**, 104029 (2004)
36. I. Navarro, J. Santiago, JHEP **02**, 007 (2005)
37. N. Barbosa-Cendejas, A. Herrera-Aguilar, JHEP **10**, 101 (2005)
38. D. Bazeia, A.R. Gomes, L. Losano, Int. J. Mod. Phys. A **24**, 1135 (2009)
39. Y.X. Liu, Y. Zhong, Z.H. Zhao, H.T. Li, JHEP **06**, 135 (2011)
40. D. Bazeia, L. Losano, R. Menezes, G.J. Olmo, D. Rubiera-Garcia, Eur. Phys. J. C **75**(12), 569 (2015)
41. Z.G. Xu, Y. Zhong, H. Yu, Y.X. Liu, Eur. Phys. J. C **75**(8), 368 (2015)
42. W.T. Cruz, L.J.S. Sousa, R.V. Maluf, C.A.S. Almeida, Phys. Lett. B **730**, 314 (2014)
43. W.D. Guo, Q.M. Fu, Y.P. Zhang, Y.X. Liu, Phys. Rev. D **93**, 044002 (2016)
44. J. Wang, W.D. Guo, Z.C. Lin, Y.X. Liu, Phys. Rev. D **98**, 084046 (2018)
45. K. Yang, W.D. Guo, Z.C. Lin, Y.X. Liu, Phys. Lett. B **782**, 170 (2018)
46. W.D. Guo, Y. Zhong, K. Yang, T.T. Sui, Y.X. Liu, Phys. Lett. B **800**, 135099 (2020)
47. F.M. Belchior, A.R.P. Moreira, R.V. Maluf, C.A.S. Almeida, Phys. Lett. B **843**, 138029 (2023)
48. A.R.P. Moreira, F.M. Belchior, R.V. Maluf, C.A.S. Almeida, Eur. Phys. J. Plus **138**(8), 730 (2023)
49. A.R.P. Moreira, F.M. Belchior, R.V. Maluf, C.A.S. Almeida, Eur. Phys. J. C **83**(1), 48 (2023)
50. F.M. Belchior, A.R.P. Moreira, R.V. Maluf, C.A.S. Almeida, Eur. Phys. J. C **83**(5), 388 (2023)
51. C.A.S. Almeida, M.M. Ferreira Jr., A.R. Gomes, R. Casana, Phys. Rev. D **79**, 125022 (2009)
52. J. Yang, Y.-L. Li, Y. Zhong, Y. Li, Phys. Rev. D **85**, 084033 (2012)
53. K. Yang, W.D. Guo, Z.C. Lin, Y.X. Liu, Phys. Lett. B **782**, 170–175 (2018)
54. A.R.P. Moreira, J.E.G. Silva, C.A.S. Almeida, Eur. Phys. J. C **81**(4), 298 (2021)
55. S. Randjbar-Daemi, M.E. Shaposhnikov, Phys. Lett. B **492**, 361–364 (2000)
56. Y.X. Liu, J. Yang, Z.H. Zhao, C.E. Fu, Y.S. Duan, Phys. Rev. D **80**, 065019 (2009)
57. Y.X. Liu, H.T. Li, Z.H. Zhao, J.X. Li, J.R. Ren, JHEP **10**, 091 (2009)
58. Y.X. Liu, L.D. Zhang, L.J. Zhang, Y.S. Duan, Phys. Rev. D **78**, 065025 (2008)
59. Y.X. Liu, C.E. Fu, L. Zhao, Y.S. Duan, Phys. Rev. D **80**, 065020 (2009)
60. Y.X. Liu, L.D. Zhang, S.W. Wei, Y.S. Duan, JHEP **08**, 041 (2008)
61. Y.N. Obukhov, J.G. Pereira, Phys. Rev. D **67**, 044016 (2003)
62. S.C. Ulhoa, A.F. Santos, F.C. Khanna, Gen. Relativ. Gravit. **49**, 54 (2017)
63. D.M. Dantas, J.E.G. Silva, C.A.S. Almeida, Phys. Lett. B **725**, 425–430 (2013)
64. L.J.S. Sousa, C.A.S. Silva, D.M. Dantas, C.A.S. Almeida, Phys. Lett. B **731**, 64–69 (2014)
65. D.M. Dantas, D.F.S. Veras, J.E.G. Silva, C.A.S. Almeida, Phys. Rev. D **92**, 104007 (2015)
66. Y.Y. Li, Y.P. Zhang, W.D. Guo, Y.X. Liu, Phys. Rev. D **95**(11), 115003 (2017)
67. H. Guo, L.L. Wang, C.E. Fu, Q.Y. Xie, Phys. Rev. D **107**(10), 104017 (2023)
68. A.R.P. Moreira, J.E.G. Silva, C.A.S. Almeida, Ann. Phys. **442**, 168912 (2022)
69. J.E.G. Silva, R.V. Maluf, G.J. Olmo, C.A.S. Almeida, Phys. Rev. D **106**(2), 024033 (2022)
70. C.E. Shannon, Bell Syst. Tech. J. **27**, 379 (1948)
71. W. Beckner, Ann. Math. **102**, 159 (1975)
72. I. Bialynicki-Birula, J. Mycielski, Commun. Math. Phys. **44**, 129 (1975)
73. Q. Tan, W.D. Guo, Y.P. Zhang, Y.X. Liu, Eur. Phys. J. C **81**(4), 373 (2021)